

Variation of Deformation Conditions of Zagros Suture Zone between Baneh and Shahrekord Areas, Iran

F. Ghahremani and A. Yassaghi*

*Department of Geology, Faculty of Basic Sciences, Tarbiat Modares University, Tehran, Islamic
Republic of Iran*

Received: 26 April 2022 / Revised: 6 May 2023 / Accepted: 31 May 2023

Abstract

Suture zones within continental collision zones generally considered as deep-seated thick-skinned thrusts/shear zones rooted in lower crust. Main Zagros Revers Fault (MZRF) is the suture zone for continental collision between the Afro-Arabia and Eurasia plates. The fault comprises of a main thrust in its NW part (Baneh area) while is partitioned to four fault splays in its SE part (Shahrekord area). Evaluation of deformation conditions of the MZRF fault rocks carried out using quartz, feldspar and calcite twins' microstructures as well as mineral composition indicates that the fault has propagated from various conditions correspond to different brittle to brittle-ductile transition zones. This implies localization and partitioning of deformation along strike of the Zagros suture zone. In the Baneh area, the suture zone is an emerged deep-rooted ductile zone, while in the Shahrekord area, this zone is detached at a basal detachment zone between basement and cover and then partitioned into four fault splays through its propagation to the upper structural level. This show that suture zones in orogenic belts might have changes along strike from thick-skinned to thin-skinned thrusts.

Keywords: Zagros suture zone, Microstructures, Deformation partitioning, Deformation conditions.

Introduction

Orogenic belts are resulted from plate convergence involving collision and suturing of continental margins (1). The lithosphere strongly deformed along these margins referred to "suture zones" where fragments of downgoing oceanic crust and mantle are also accommodated (2). A complex deformation including strong partitioning of deformation conditions and kinematics are common in these zones (3). Deformation conditions data provide important constraints in understanding the tempo-spatial evolution of orogenic belts (4, 5). Such data can also be used as a powerful

tool to determine the burial and exhumation history during continental thickening episodes (6).

Microstructural studies have always been one of the qualitative ways for analyzing the conditions of deformation (7, 8). The Zagros suture zone along which discrete outcrops of ophiolite rocks exist, resulted from continental convergence of Afro-Arabia with Eurasia plates (9-11). Disparity of the suture zone's fault rocks from cataclasite to mylonite (12) implies variation on its deformation conditions. This study attempts to present field data as well as mineral composition and microstructures of the suture zone rocks to constrain the nature and conditions of the Zagros collision zone. This

* Corresponding Author: Tel: +98 21 8288 3406; Email: Yassaghi@modares.ac.ir

could provide key to investigate inequality on deformation conditions of younger orogenic belts.

Geological setting

Zagros orogeny started with obduction of Neotethys oceanic crust over the Afro-Arabian Plate in the Late Cretaceous (9, 13-15). The orogeny then followed by Early Miocene continental–continental collision of the plate with the central Iran (16-19). The collision is characterized by an oblique orogeny resulted in deformation partitioning across the convergence zone among the internal metamorphic zone, the external fold-and-thrust belt, and their suture zone (20-24). The Main Zagros Reverse Fault (MZRF) suturing the Afro-Arabian passive continental margin (Zagros fold-thrust belt to the southwest) with the central Iran (active continental margin to the northeast), as a southern edge of the Eurasia Plate (10, 25-27) (Fig. 1). The MZRF is a major distinct fault in the Zagros NW part (Fig. 1c), along which discrete masses of the obducted ophiolite of the Neotethyan oceanic crust remnant crops out is considered as the Zagros suture zone and fault rocks

from the MZRF derive from below the seismogenic zone (less than 20 km) (11) (Fig. 2b). In the Zagros SE part, however, the MZRF comprises several oblique faults as the Ben, Hafshejan, Farsan and Ardal faults. Nemati and Yassaghi (28) consider these faults display duplex thrust system and converge at depth to form a crustal scale thrust, considered as the root zone of the Zagros orogen (Figs. 1d, 4). The younger and active Main Recent Fault (MRF) cuts the MZRF (Fig. 1).

Materials and Methods

The used data in this study are field mapping of the structures within the MZRF zones as well as sampling of the zones fault core for the study of their main minerals microstructures and X-ray analysis. The area under investigation are the Baneh (in the NW part of the MZRF) and Shahrekord (in the SE part of the MZRF) (Figs. 2 and 4). To decipher the kinematics of the zones, their movement directions and senses were interpreted using shear lenses from which S–C fabric/structures (29) are acquired (Figs 3 and 5). Sampling carried out

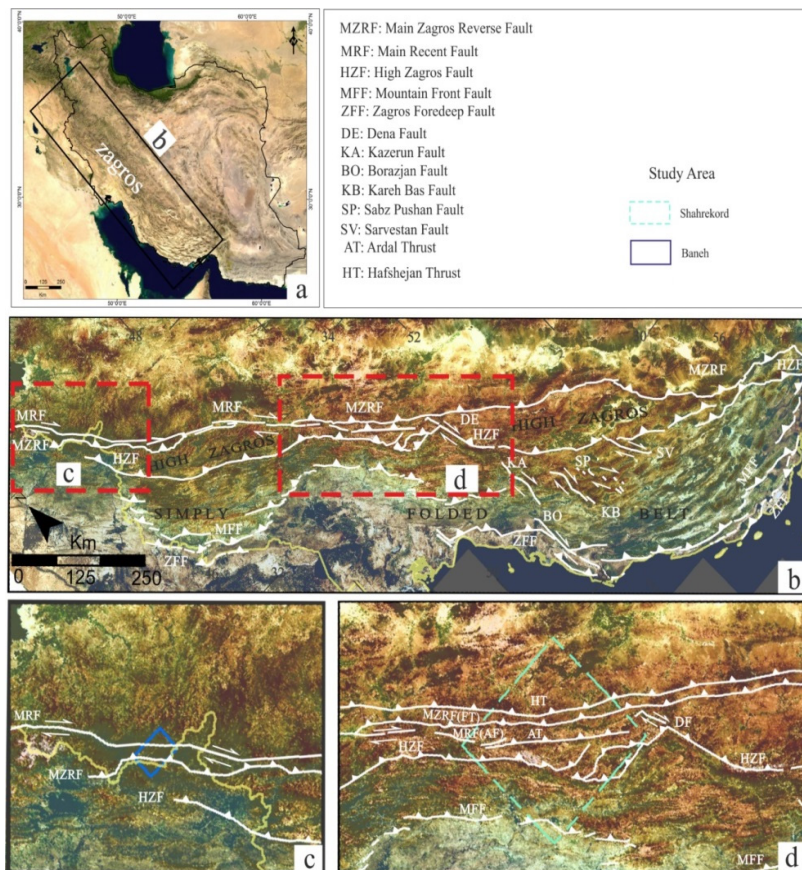


Figure 1. (a): Shows the location of Zagros within the Arabia-Eurasia convergent zone. (b): The main Zagros faults. Location of the studied areas in (c) (Baneh area, blue rectangle) and (d) (Shahrekord area, dashed green rectangle).

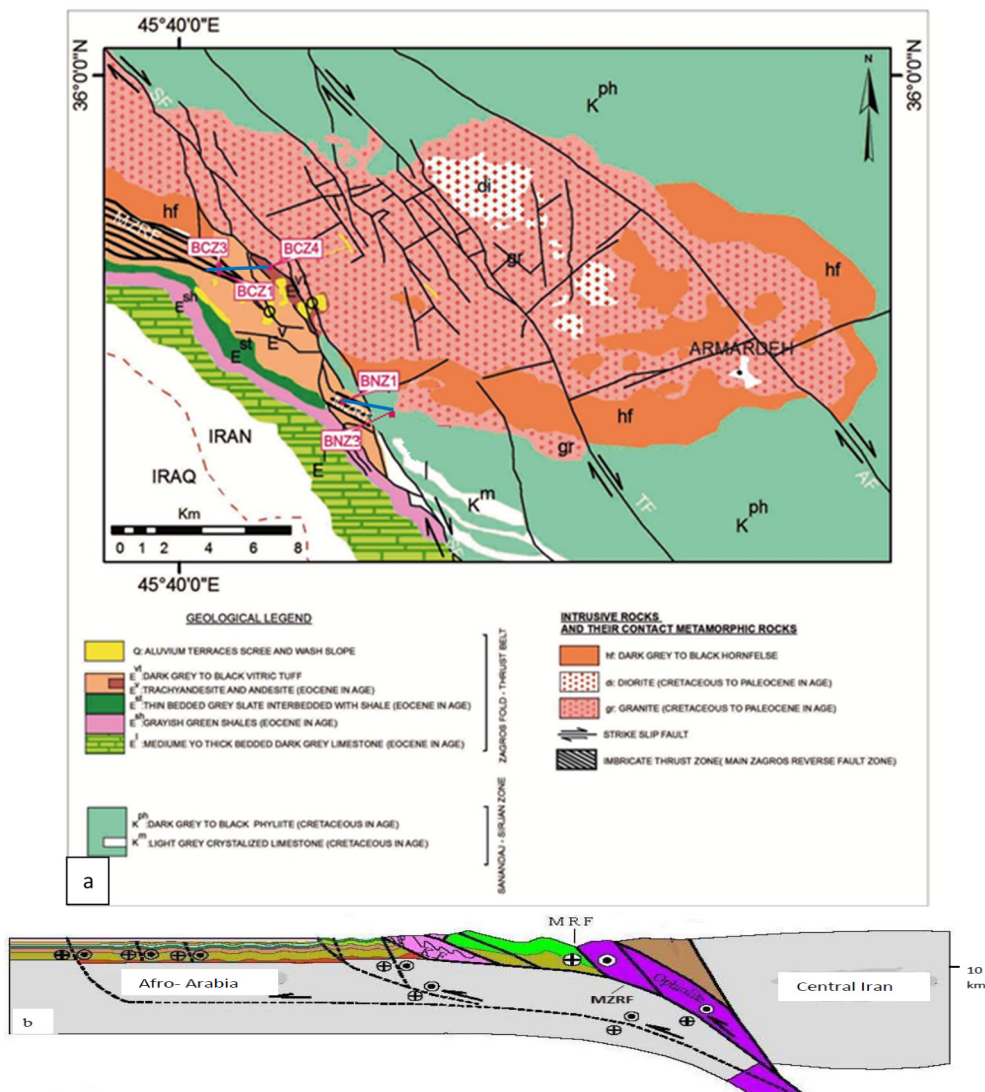


Figure 2. (a): Map of the Baneh area [after 44] indicates location of the investigated samples along the MZR as the BCZ1, BCZ3 and BCZ4 in the northern part (the Choman section) and the BNZ1 and BNZ3 in the southern part (the Nirvan section) of the area. (b): Sketch section of the Zagros suture zone in the Baneh area showing the location of the MZR derive from depth more than 15 km [after 11].

based on the quality of the exposure and accessibility to the fault core where observable degree of fabric development increased. We collected five samples from the Baneh area (Fig. 2) and three samples from the Shahrekord area (Fig. 4). Microstructures as well as petrography of the samples were studied in the XZ plane, of the finite strain ellipse, of their thin sections, with the aim of investigating the deformational behavior of quartz, feldspar and calcite minerals (Table 1).

Conventional powder X-ray diffraction (XRD) was also performed on all the fault rock samples to quantify their mineral compositions and proportions and the results are presented in Table 2. All interpretation was

performed using TOPAS software from Bruker AXS1. TOPAS performs a Rietveld refinement on the diffraction pattern resulting in a modeled diffraction pattern that closely matches the original data (30).

Results

In this section, detailed microstructural studies on quartz, feldspar and calcite minerals of the selected samples along the MZR (Fig. 1) as well as their composition are presented.

Microstructural observations

Baneh area: In northern part of Baneh area in which

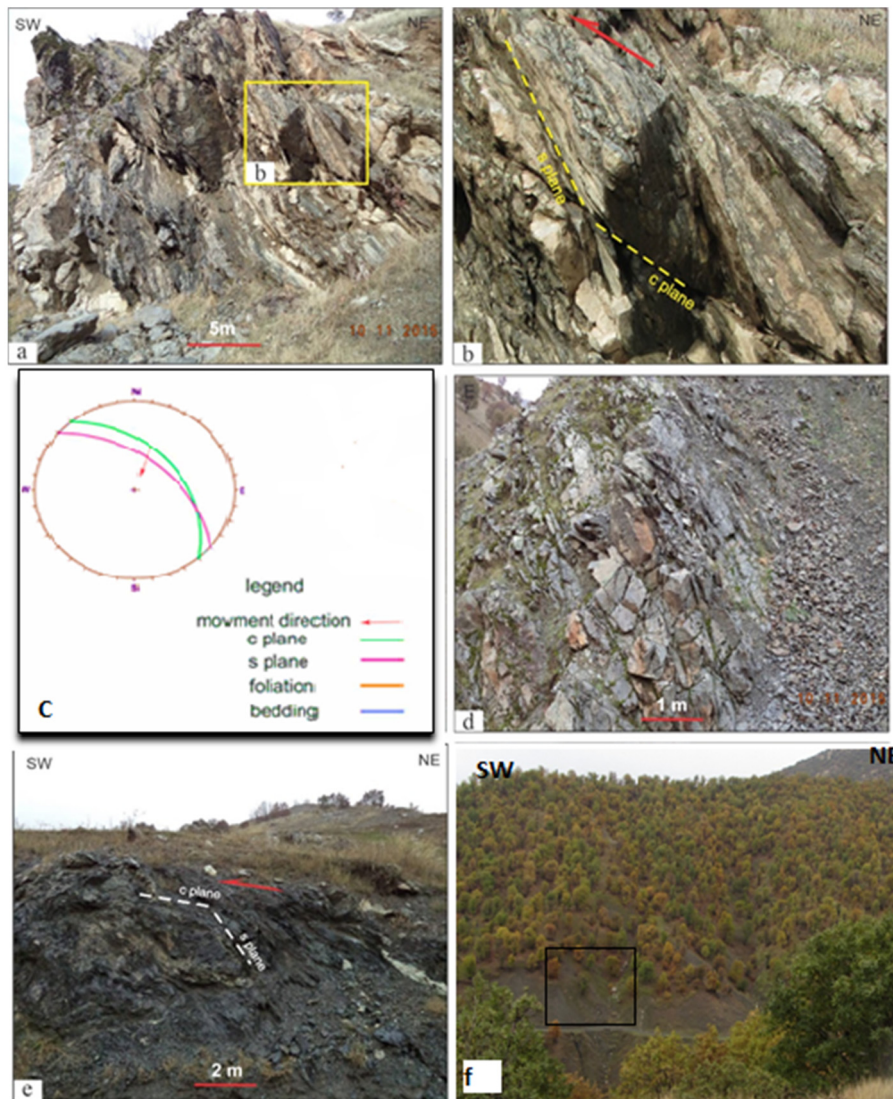


Figure 3. The MZRF zone in the Baneh area (a, b, and d are the outcrops of the MZRF in northern part, e and f are the outcrops of the fault southern part). (a) and (b): Show development of S-C structures in volcanic rocks where the BCZ3 sample is taken. (c): Lower hemisphere equal area stereographic projection of the S-C structures in the MZRF zone in the Baneh area. (d): Location of the sample BCZ4 taken from 1 kilometer far from the sample BCZ3 on the hanging wall of the MZRF. (e): Outcrop of ophiolite rocks along the MZRF where the BNZ1 sample is taken. (f): Location of the sample BNZ3 collected from the MZRF footwall.

the MZRF comprises of a sole mega-thrust, microstructural investigation on three selected samples (BCZ1, BCZ3 and BCZ4 in Fig. 2) all are Eocene Andesite and trachyandesite rocks is performed. The BCZ1, BCZ3 samples are collected from the fault core (Figs. 2 and 3). The modal analyses of these samples show quartz (~80%), feldspar (~15%) and very small amounts of Clay minerals (Muscovite and chlorite) (~5 %). In the BCZ1, BCZ3 samples, quartz grains show intracrystalline deformation features such as undulose

and sweeping undulatory extinction as well as subgrain microstructures (Fig. 6a, b). Intercrystalline deformation in the form of low temperature grain boundary migration or bulging (BLG) recrystallization has also worked well in these quartzs resulted in development of new and small grains on margin of the old grains to form core-and-mantle structure (Fig. 6a, b and Table 1). The observed feldspar microstructures (e.g., in BCZ1 sample, Table 1) include intracrystalline fracturing (Fig. 6c, d) in almost half of the grains (Fig. 6f), and slightly

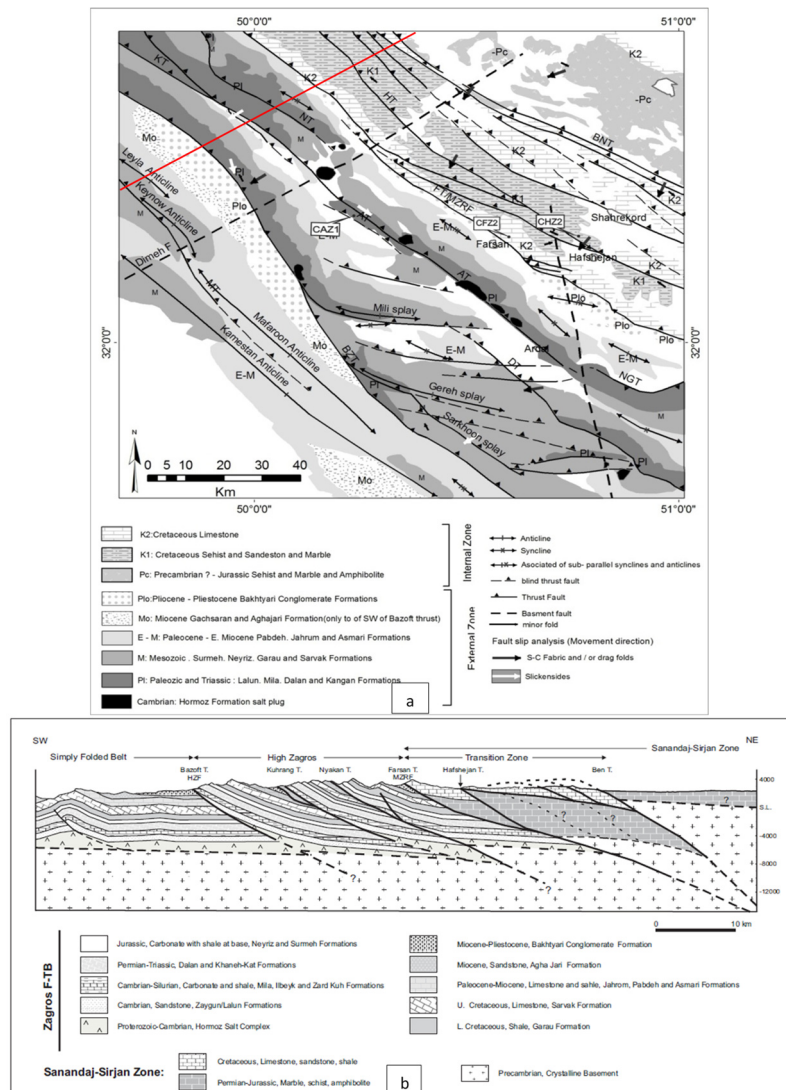


Figure 4. (a): Structural map of the Shahrekord area [after 28] show the location of samples taken from the MZRF and MRF fault zones. MT: Mafaroon thrust, BZT: Bazoft thrust, DP: Dopolan thrust, KT: Kuhrang thrust, AT: Ardal thrust, NGT: Naghan thrust, NT: Nyakan thrust, FT: Farsan thrust, HF: Hafshejan thrust and BNT: Ben thrust. Note to location of the studied samples (CAZ1, CFZ2, and CHZ2). (b): Structural cross section across the High Zagros Zone at Bakhtyari area [after 28], the red line in (a) is the location of the cross section.

Fig 4. (a): Structural map of the Shahrekord area [after 28] show the location of the studied samples (CAZ1, CFZ2, and CHZ2). (b): Structural cross section across the High Zagros Zone at Bakhtyari area [after 28], the red line in (a) is the location of the cross section.

undulatory extinction deformation twins (Fig. 6e) and bent twins (Fig. 6d) in the rest of grains. The rock foliation exhibits subtle sigmoidal shapes, comprising the S-C fabric (Fig. 6g, h in BCZ3 sample). Chlorite grains are deformed to develop undulose extinction and Mica fish (Fig. 6g).

The BCZ4 rock sample is taken from the Eocene vitric tuff (Fig. 2) ~1km to the W of the MZRF core. Quartz grains in this sample show intracrystalline deformation features such as undulose and sweeping

undulatory extinction as well as subgrain microstructures (Table 1). Intercrystalline deformation in the form of low temperature grain boundary migration or bulging (BLG) recrystallization have seen in less than 2% of quartz grains. Less than 5 % of feldspar grains are deformed to develop intracrystalline fractures along which more of them solubilized to sericite (Fig. 6I, j). Muscovite grains tends to resist deformation and few of them develop into Mica fish (Fig. 6k).

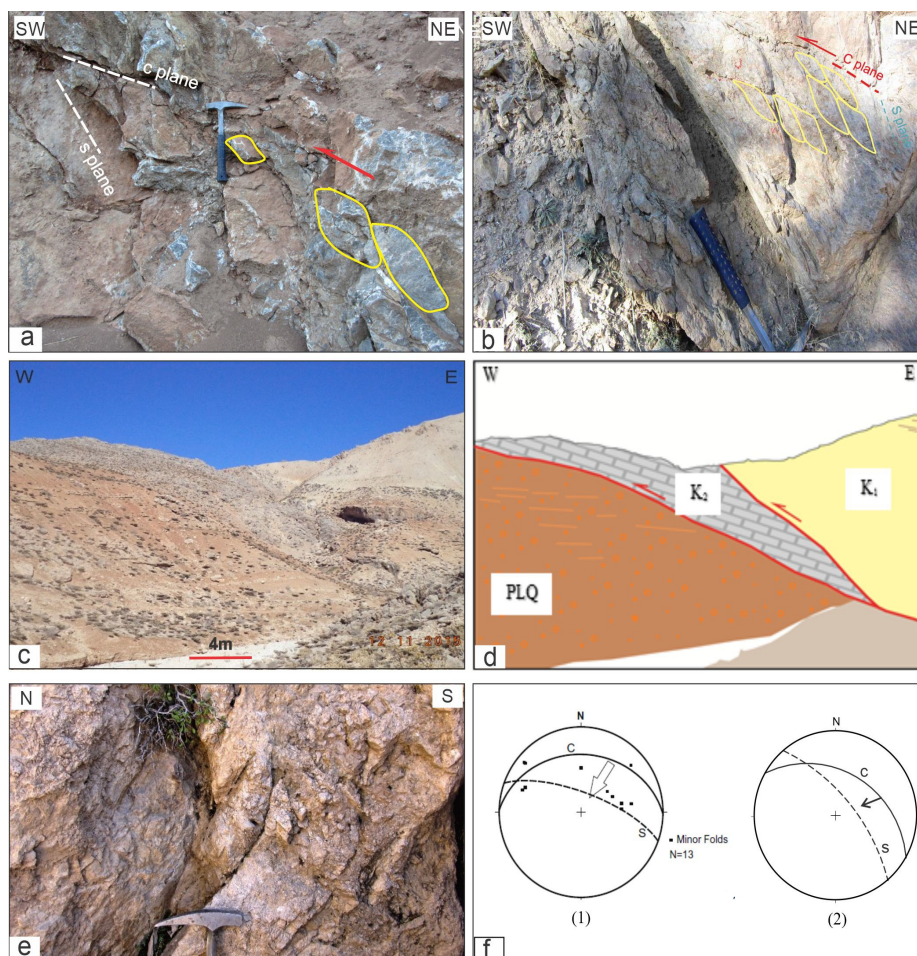


Figure 5. (a): The Hafshejan fault zone where the CHZ2 sample is collected. Note to S-C structures in Cretaceous carbonate rocks through which the lensoidal fault rocks have developed. (b): The Farsan fault zone in Cretaceous carbonate rocks from which the CFZ2 sample is collected. (c) and (d): The Ardal fault zone along which Cretaceous carbonate (K_2) and Marl (K_1) thrust over the Pleistocene Bakhtyari conglomerate. (e): The Ardal fault zone where the CAZ1 sample is collected. (f): Lower hemisphere equal area stereographic projection of structures in (1) the Hafshejan and (2) the Farsan fault zones that show southwestward sense of shear. Refer to Fig. 4 for the samples locations.

In southern part of the Baneh area, the BNZ1 sample was taken from the MZRF fault core whereas the BNZ3 sample was collected from the fault damage zone (Fig. 2). Since the BNZ1 sample is mainly composed of tiny phyllosilicate minerals (more likely from chemical alteration of original pyroxene and amphibole), the developed microstructure is only crenulation cleavage (Fig. 6l, m). The BNZ3 sample is mainly composed of quartz grains and some muscovite minerals that have not been deformed (Fig. 6n).

Shahrekord area: The MZRF in this area comprises four fault zones as the Ben, Hafshejan (the CHZ2 sample as Cretaceous sandstone), Farsan (the CFZ2 sample as Cretaceous limestone) and Ardal (the CAZ1 sample as Cretaceous limestone) faults from northeast to southwest (Fig. 4). In the Hafshejan fault zone, lensoidal fault rock in which S-C structure are formed

show brittle-ductile conditions for the fault (Fig. 5a). Investigation on microstructure of the fault rock sample (Fig. 4 and Table 1) shows almost all quartz grains are deformed to intracrystalline fractures, along which solubilization to sericite are present (Fig. 7a), as well as undulose and sweeping undulatory extinction (Fig. 7a). Only 15% of quartz grains deformed to develop subgrain (Fig. 7c) and less than 5% of them deformed to intercrystalline low temperature grain boundary migration or bulging (BLG) recrystallization (Fig. 7b and Table 1).

Evaluation of calcite twins in the CFZ2 and CAZ1 samples (Figs. 4 and 5b, e) using criteria of Burkhard (7) and Ferrill et al (31) show that they are deformed to types I, II and III mechanical twins (Fig. 7e, f and Table 1). In these samples, development of stylolitic fractures represents the action of pressure solution

Table 1. Microstructure of the MZRF Rocks

| Area | Sample | Microstructure | |
|-------------------------|--------------|--|--|
| 1.Choman section | BCZ1 | Quartz minerals: undulose extinction>90%, sweeping extinction~55-60%, subgrain~35-40%, core and mantle structure feldspar minerals: intracrystalline fractures>50%, undulose extinction<15%, deformation twins and bent twins~5-10% | |
| | BCZ3 | Quartz minerals: undulose extinction~100%, sweeping extinction~60-65%, subgrain~40-45% feldspar minerals: intracrystalline fractures>50% | |
| | Baneh | BCZ4 | Quartz minerals: undulose extinction~75-80%, sweeping extinction~30-35%, subgrain~15-20% feldspar minerals: intracrystalline fractures<5% |
| | | 2.Nirvan section | BNZ1 |
| | BNZ3 | No deformed | |
| Shahrekord | CHZ2 | Quartz minerals intracrystalline fractures>85%, undolose extinction~70%, sweeping extinction~20%, subgrain~15%, bulging<5% | |
| | CFZ2 | Calcite twin type I~48%, type II~52% | |
| | CAZ1 | Calcite twin type I~50%, type II~45%, type III<5% | |

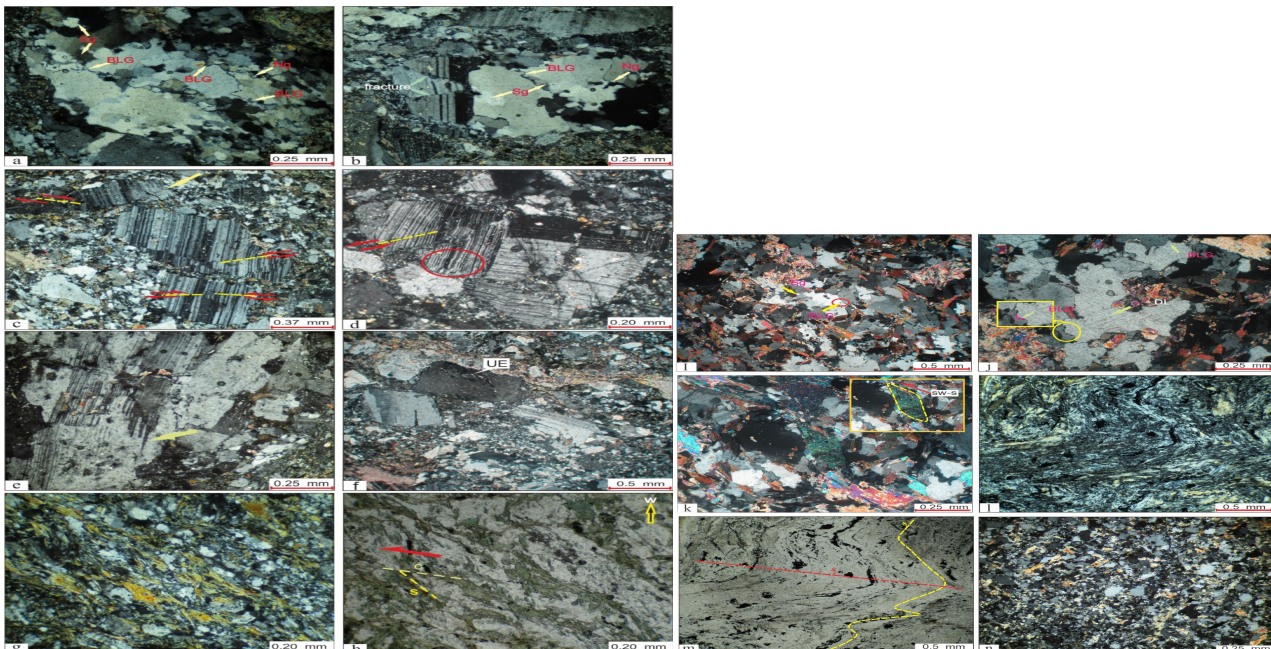


Figure 6. Microstructure of the MZRF rocks in the Baneh area. (a) and (b): Quartz microstructures (BCZ1 sample) (Sg: subgrain, Ng: new grain, BLG: bulging as low grade temperature recrystallization) show initial development of core and mantle structure while feldspar grains show intracrystalline fractures in image (b). (c) and (d): Fractures and bending in feldspar grains in BCZ1 sample (arrow in image c and ellipse in image d). (e): Deformation twins in feldspar grains of the BCZ1 sample (arrow). (f): Undulose extinction in feldspar grains of sample BCZ1. (g) and (h): S-C fabric deduced from mica fishes in the BCZ3 sample, arrow shows the sense of movement (g: xpl, h: ppl). (i) and (j): Quartz microstructures (BCZ4 sample) (Sg: subgrain, DL: Deformation lamellae, BLG: bulging as low grade temperature recrystallization). (k): Mica fish in the sample BCZ4. (l) and (m): Crenulation cleavage (S_2 as red dashed line) in the sample BNZ1 (l: xpl, m: ppl). (n): Photomicrograph of the BNZ3 sample show undeformed grains.

deformation mechanism (Fig. 7d).

Rock composition

X-ray diffraction analysis carried out on selected samples from the MZRF show that major mineral assemblages of the BNZ1 sample (Fig. 2) is chrysotile (43.4%), Lizardite (49.4%) and Magnetite (7.2%)

(Table 2, Fig. 8a). Lizardite and chrysotile is believed as the result of serpentinization proceeded from olivine and orthopyroxene (32) that is the main mineral of ophiolites. However, the BNZ3 sample (Fig. 2) is composed of Quartz (51%), Muscovite (23%), Albite (16.2%) and Clinocllore (9.7%). The CAZ1 and CFZ2 samples gathered from the Farsan and Aradal Fault

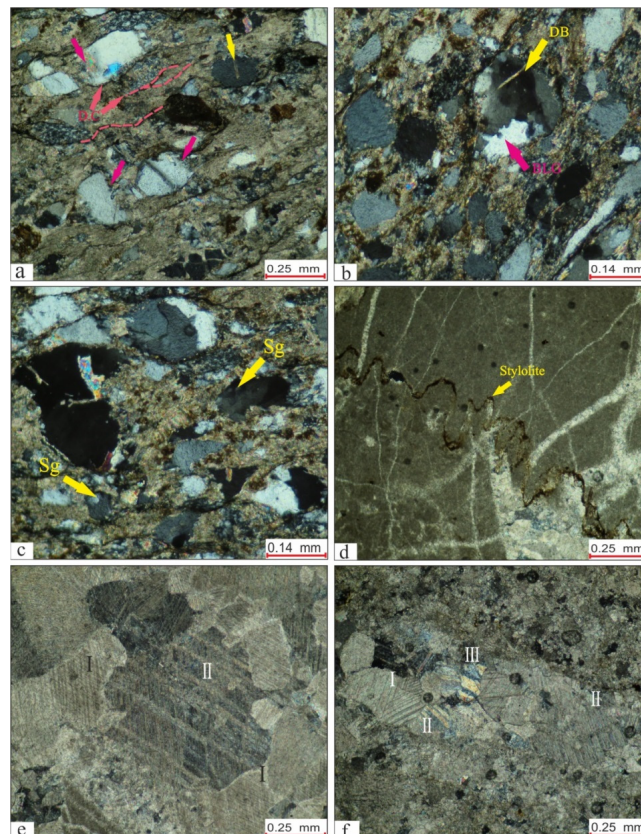


Figure 7. Microstructure of the MZRF rocks in the Shahrekord area. (a), (b), and (c): Quartz microstructure in the sample CHZ2. (a): Show development of fractures (yellow arrow) and solution cleavages in quartz grains (pink arrow) as well as disjunctive cleavage (red dashed curves). (b): Deformation band (DB) and bulging recrystallization (BLG) in quartz. (c): Subgrain (sg) in quartz. (d): Stylolite structures in calcite grains. (e) and (f): Mechanical twins in calcite grains in the samples CFZ2 and CAZ1, respectively. Refer to Fig. 4 for the samples locations.

zones in the Shahrekord area generally composed of carbonate minerals. The CAZ1 sample is composed of Calcite (14.9%), Dolomite (84.3%), Quartz (0.3%) and Albite (0.5%) whereas the CFZ2 sample is comprises calcite mineral (~100%) (Table 2 and Fig. 8b).

Discussion

The developed microstructures in the quartz and feldspar minerals of the MZRF rocks in the Baneh area (Fig. 6) represents that the fault rocks are deformed as low-grade mylonite. The quartz is usually deformed by crystal-plastic processes as shown by its change in shape and by its intracrystalline undulose extinction as well as grain boundary Bulging (Fig. 6a, b). As Trouw et al (33) suggested these quartz microstructures is common in low-grade mylonites. The feldspar grains, however, deform by fracturing (Fig. 6c, d). The phyllosilicate minerals tends to resist deformation and may develop into porphyroclastic "fish", especially when surrounded by quartz (Fig. 6g, h). The quartz microstructures correspond to the lower part of regime 2

by Hirth and Tullis (34) and BLG II by Stipp et al (35) and that deformation temperature of the fault rock is approximately 350°C (Fig. 9a) while microstructures of the feldspar minerals correspond to temperature lower than 400°C (36).

The temperature range for low-grade mylonites is thought to be roughly between 250 and 500°C (33). According to the microstructures of the quartz and feldspar minerals in samples from the Baneh area, the MZRF is deformed under temperature of about 400 °C. Assuming a geothermal gradient of 26 °C/km equal to adiabatic condition, this temperature represent the depth of ~15 km for formation of the suture zone. For crustal rocks made of granitic (quartz and feldspar bearing) the brittle-ductile transition occurs in the range of 10-15 km (37). This depth is correspond to the depth of the ophiolite rocks emplaced over the Arabian Platform as passive continental margin during the obduction of the the Neotethys oceanic crust in the Late Cretaceous to early Paleocene (9, 14, 15). In addition, X-ray diffraction analysis on the rock sample (BNZ1) from the

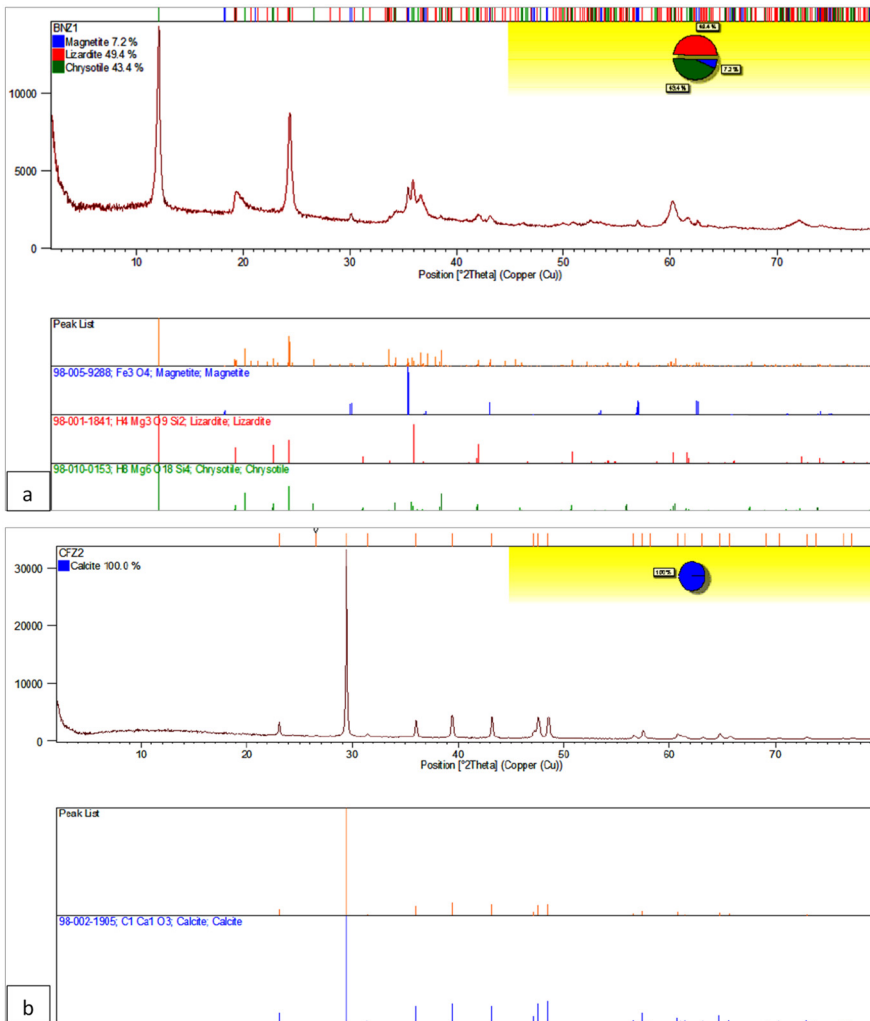


Figure 8. (a): X-ray diffraction pattern of the sample BNZ1 show chrysotile, lizardite and magnetic peaks as its main minerals. (b): X-ray diffraction pattern of sample CFZ2 show only calcite mineral.

MZRF in the Baneh area (Fig. 8) show that this rock consist of serpentine group minerals. Serpentine minerals generally form by hydration of mafic and ultramafic rocks like ophiolites and in temperature from 300 to 500 °C (38, 39), which is correspond to low grade mylonites prosed here for the conditions of the MZRF fault rock in the Baneh area. Thus, the MZRF in this area is a deep-rotted thrust along which emplacement of the ophiolitic rocks to the upper structural level occurred in a brittle-ductile transition condition.

Quartz mineral microstructures of the MZRF in the Sharekord area (the CHZ2 sample in Table 1 and Fig. 7) where it comprises several fault zones (Fig. 4) represent deformation correspond to regime 1 by Hirth and Tullis (34) and BLG I by Stipp et al (35). The deformation temperature is thus equal to 300 °C (Fig. 9a). Similarly,

evaluation of calcite twins in calcite minerals (the CFZ2 and CAZ1 samples in Table 2 and Fig. 7) based on Burkhard (7) and Ferrill et al (31) criteria show that they generally deformed to type I and type II mechanical twins correspond to deformation temperature of about 250°C (Fig. 9b). Thus, according to the microstructures of quartz and calcite minerals, it can be proposed that the MZRF fault zones in this area is deformed under temperature of about 300 °C. Assuming a geothermal gradient of 26° C/km equal to adiabatic condition, this temperature represent the depth of 10 km for the formation of these fault zones in a brittle conditions.

Comparison of microstructures as well as rock composition of the studied samples indicates that in the Baneh area the Zagros suture zone is spatially localized along a main deep rotted ductile thrust originated from the depth correspond to brittle-ductile deformation

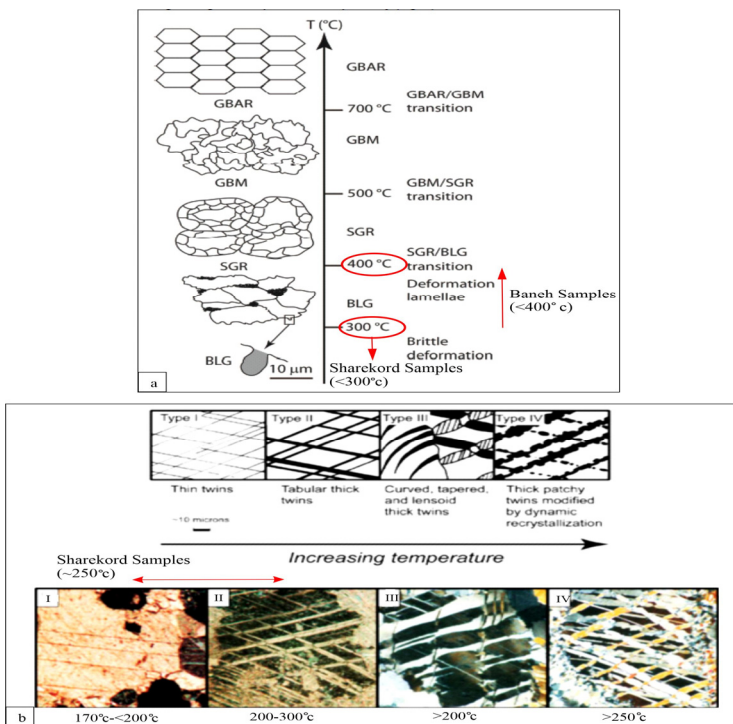


Figure 9. Schematic diagrams illustrating the ranges of temperature of (a): the three dynamic recrystallization mechanisms of quartz (BLG (bulging low grade), SGR (subgrain rotation), GBM (grain boundary migration) and GBAR (grain boundary area reduction)) [after 35, 36, 45]. (b): Twin morphology in calcite [after 7, 31].

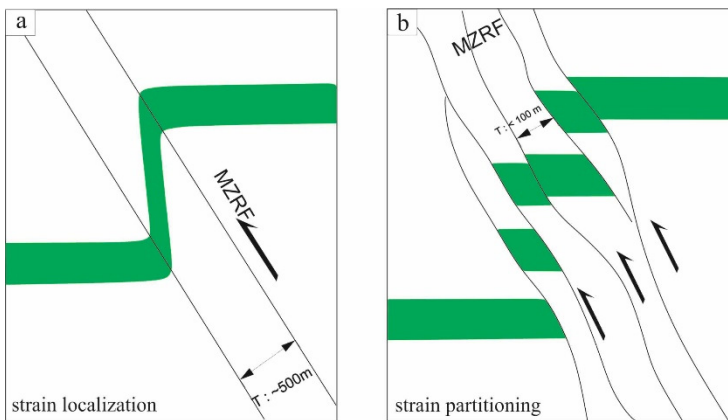


Figure 10. Cross section showing localization and partitioning of deformation along the MZRF in (a): Baneh area, (b): Shahrekord area.

condition. In the Shahrekord area, however, the suture zone is spatially partitioned into several thrust splays rooted at depth to a deeper megathrust (Fig. 10).

It is generally believed that the MZRF is a paleo-structure related to the Proterozoic basin (40) that extend in an extensional rift basin (41) related to the Neo-Tethys rifting (42). During Miocene-Pliocene, as consequence of Zagros shortening synchronous to development of Zagros Fold thrust belt, the paleo-extensional fault has reactivated to an inverted normal

fault. We believe that through this fault inversion the NW part of the MZRF inverted through preexisting normal fault to form a deep-rotted thick-skinned thrust whereas the fault SE part is inverted as footwall shortcut thrust through a detachment zone between basement and cover (43). This detachment fault then propagated to the surface as imbricate thin-skinned thrusts (i.e., the Ben, Hafshejan and Farsan thrusts in Fig. 4).

Conclusion

Microstructural studies on selected samples across the Zagros suture zone indicate that the zone is deformed under different deformation conditions. In the Shahrekord area, the fault rocks come from within the seismogenic zone (under temperature of about 300 °C and depth of 10 km) and indicate brittle deformation condition. In the Baneh area, the fault rocks derive from below the seismogenic zone (under temperature of about 400 °C and depth of ~15 km) and indicate brittle to brittle-ductile transition conditions. In addition, X-ray diffraction results on samples from this area show that these rocks are serpentinized ophiolites correspond to low grade mylonite deformation. Spatial development of the ophiolite rocks in the Baneh area indicates localization of the suture zone deformation along a basement involved ductile thrust. In the Shahrekord area, however, the suture zone is partially detaches at the basement-cover and imbricated thrust splays propagated to the surface. This indicates that an emerged suture zone to the surface in orogenic belts might have changes along strike from thick-skinned megathrust to thin-skinned imbricated thrusts.

References

1. Van der Pluijm BA, Marshak S. Earth structure: an introduction to structural geology and tectonics; 1997.
2. Şengör, ACl. Plate tectonics and orogenic research after 25 years: A Tethyan perspective. *Earth-Science Reviews*. 1990;27(1-2):1-201.
3. Braudy N, Gaschnig R, Wilford D, Vervoort J, Nelson C, Davidson C, et al. Timing and deformation conditions of the western Idaho shear zone, West Mountain, west-central Idaho. *Lithosphere*. 2017; 9 (2):157-83.
4. Barr TD, Dahlen F. Brittle frictional mountain building: 2. Thermal structure and heat budget. *Journal of Geophysical Research: Solid Earth*. 1989; 94 (B4):3923-47.
5. Karabinos P, Ketcham R. Thermal structure of active thrust belts. *Journal of Metamorphic Geology*. 1988; 6 (5):559-70.
6. Vityk MO, Bodnar RJ, Dudok IV. Fluid inclusions in "Marmarosh Diamonds": evidence for tectonic history of the Folded Carpathian Mountains, Ukraine. *Tectonophysics*. 1996; 255 (1-2):163-74.
7. Burkhard M. Calcite twins, their geometry, appearance and significance as stress-strain markers and indicators of tectonic regime: a review. *Journal of structural geology*. 1993; 15 (3-5):351-68.
8. Tullis J, Yund RA. Diffusion creep in feldspar aggregates: experimental evidence. *Journal of Structural Geology*. 1991; 13 (9):987-1000.
9. Agard P, Omrani J, Jolivet L, Whitechurch H, Vrielynck B, Spakman W, et al. Zagros orogeny: a subduction-dominated process. *Geological Magazine*. 2011; 148 (5-6):692-725.
10. Berberian M, King G. Towards a paleogeography and tectonic evolution of Iran. *Canadian journal of earth sciences*. 1981; 18 (2):210-65.
11. Sadeghi S, Yassaghi A. Spatial evolution of Zagros collision zone in Kurdistan, NW Iran: Constraints on Arabia–Eurasia oblique convergence. *Solid Earth*. 2016; 7 (2):659-72.
12. Yassaghi A, Marone C. The relationship between fault zone structure and frictional heterogeneity, insight from faults in the High Zagros. *Tectonophysics*. 2019; 762:109-20.
13. Gidon M, Berthier F, Billiaut J, Halbronn B, Maurizot P. Sur quelques caractères de la tectonique néocrétacée dans la région de Borudjerd (Zagros oriental, Iran). *Comptes Rendus de l'Académie des Sciences*. 1974; 278(Série D):577.
14. Karim KH, Koyi H, Baziany MM, Hessami K. Significance of angular unconformities between Cretaceous and Tertiary strata in the northwestern segment of the Zagros fold–thrust belt, Kurdistan Region, NE Iraq. *Geological Magazine*. 2011; 148(5-6):925-39.
15. Kazmin V, Ricou L-E, Sbertshikov I. Structure and evolution of the passive margin of the eastern Tethys. *Tectonophysics*. 1986; 123(1-4):153-79.
16. Allen MB, Armstrong HA. Arabia–Eurasia collision and the forcing of mid-Cenozoic global cooling. *Palaeogeography, Palaeoclimatology, Palaeoecology*. 2008; 265 (1-2):52-8.
17. McQuarrie N, van Hinsbergen DJ. Retrodeforming the Arabia-Eurasia collision zone: Age of collision versus magnitude of continental subduction. *Geology*. 2013; 41 (3):315-8.
18. Mouthereau F, Lacombe O, Vergés J. Building the Zagros collisional orogen: timing, strain distribution and the dynamics of Arabia/Eurasia plate convergence. *Tectonophysics*. 2012; 532: 27-60.
19. Mouthereau F, Tensi J, Bellahsen N, Lacombe O, De Boisgrollier T, Kargar S. Tertiary sequence of deformation in a thin-skinned/thick-skinned collision belt: The Zagros Folded Belt (Fars, Iran). *Tectonics*. 2007; 26 (5).
20. Allen MB, Kheirkhah M, Emami MH, Jones SJ. Right-lateral shear across Iran and kinematic change in the Arabia–Eurasia collision zone. *Geophysical Journal International*. 2011; 184 (2): 555-74.
21. Jackson J. Partitioning of strike-slip and convergent motion between Eurasia and Arabia in eastern Turkey and the Caucasus. *Journal of Geophysical Research: Solid Earth*. 1992;97(B9):12471-9.
22. Jackson J, McKenzie D. Active tectonics of the Alpine–Himalayan Belt between western Turkey and Pakistan. *Geophysical Journal International*. 1984; 77 (1):185-264.
23. Talebian M, Jackson J. A reappraisal of earthquake focal mechanisms and active shortening in the Zagros mountains of Iran. *Geophysical Journal International*. 2004; 156 (3):506-26.
24. Copley A, Jackson J. Active tectonics of the Turkish-Iranian plateau. *Tectonics*. 2006; 25 (6).
25. McQuarrie N, Stock J, Verdel C, Wernicke B. Cenozoic evolution of Neotethys and implications for the causes of plate motions. *Geophysical research letters*. 2003; 30 (20).
26. Mohajjel M, Fergusson C, Sahandi M. Cretaceous–Tertiary

- convergence and continental collision, Sanandaj–Sirjan zone, western Iran. *Journal of Asian Earth Sciences*. 2003; 21 (4):397-412
27. Takin M. Iranian geology and continental drift in the Middle East. *Nature*. 1972; 235:147-50.
28. Nemati M, Yassaghi A. Structural characteristics of the transitional zone from internal to external parts of the Zagros orogen, Iran. *Journal of Asian Earth Sciences*. 2010; 39 (3):161-72.
29. Mitra G, Marshak S. *Basic Methods of structural Geology*, Prentice–Hall. Inc, New Jersey. 1988:232-3.
30. Rietveld HM. A profile refinement method for nuclear and magnetic structures. *Journal of applied Crystallography*. 1969; 2 (2):65-71.
31. Ferrill DA, Morris AP, Evans MA, Burkhard M, Groshong Jr RH, Onasch CM. Calcite twin morphology: a low-temperature deformation geothermometer. *Journal of structural Geology*. 2004; 26 (8):1521-9.
32. Aswad KJ, Aziz NR, Koyi HA. Cr-spinel compositions in serpentinites and their implications for the petrotectonic history of the Zagros Suture Zone, Kurdistan Region, Iraq. *Geological magazine*. 2011; 148 (5-6):802-18.
33. Trouw RA, Passchier CW, Wiersma DJ. *Atlas of Mylonites-and related microstructures*: Springer Science & Business Media; 2009.
34. Hirth G, Tullis J. Dislocation creep regimes in quartz aggregates. *Journal of structural geology*. 1992; 14 (2):145-59.
35. Stipp M, Stüënitz H, Heilbronner R, Schmid SM. The eastern Tonale fault zone: a ‘natural laboratory’ for crystal plastic deformation of quartz over a temperature range from 250 to 700 C. *Journal of structural geology*. 2002; 24 (12):1861-84.
36. Passchier CW, Trouw RA. *Microtectonics*: Springer Science & Business Media; 2005.
37. Fossen H. *Structural geology*: Cambridge university press; 2010.
38. O’Hanley D. *Oxford monographs on geology and geophysics. Serpentinites Records of Tectonic and Petrological History*. 1996; 34.
39. Iyer K. *Mechanisms of serpentinization and some geochemical effects* (Ph. D. Thesis). Oslo: University of Oslo, 2007. 2007.
40. Blasband B, White S, Brooijmans P, De Boorder H, Visser W. Late Proterozoic extensional collapse in the Arabian–Nubian shield. *Journal of the Geological Society*. 2000; 157 (3):615-28.
41. Al-Husseini MI. Origin of the Arabian Plate structures: Aram collision and Najd rift. *GeoArabia*. 2000; 5 (4):527-42.
42. Sepehr M, Cosgrove J. Structural framework of the Zagros fold–thrust belt, Iran. *Marine and Petroleum geology*. 2004; 21 (7):829-43.
43. McClay K, Buchanan P. Thrust faults in inverted extensional basins. *Thrust tectonics*. 1992:93-104.
44. Sadeghi S, Yassaghi A, Fathollahi M. Structural Analysis of the Main Recent Fault and its Relation with the Main Zagros Reverse Fault in Kurdistan. *Scientific Quarterly Journal of Geosciences*. 2013; 22 (88):41-50.
45. Kruse R, Stüënitz H, Kunze K. Dynamic recrystallization processes in plagioclase porphyroclasts. *Journal of Structural Geology*. 2001; 23 (11):1781-802.